

Science

AAAS

Ab Initio Determination of Light Hadron Masses

S. Dürr, *et al.*

Science **322**, 1224 (2008);

DOI: 10.1126/science.1163233

The following resources related to this article are available online at www.sciencemag.org (this information is current as of November 21, 2008):

Updated information and services, including high-resolution figures, can be found in the online version of this article at:

<http://www.sciencemag.org/cgi/content/full/322/5905/1224>

Supporting Online Material can be found at:

<http://www.sciencemag.org/cgi/content/full/322/5905/1224/DC1>

This article appears in the following **subject collections**:

Physics

<http://www.sciencemag.org/cgi/collection/physics>

Information about obtaining **reprints** of this article or about obtaining **permission to reproduce this article** in whole or in part can be found at:

<http://www.sciencemag.org/about/permissions.dtl>

23. R. W. Romani, *Astrophys. J.* **470**, 469 (1996).
 24. P. Goldreich, W. H. Julian, *Astrophys. J.* **157**, 869 (1969).
 25. Data provided by EGRET; <http://legacy.gsfc.nasa.gov/compton/data/egret/>.
 26. F. Lucarelli *et al.*, *Nucl. Instr. Meth. A* **589**, 415 (2008).
 27. A. K. Harding, private communication.
 28. We thank the electronics division at the Max-Planck-Institut, Munich, for their work in developing and producing the analog sum trigger system, especially O. Reimann, R. Maier, S. Tran, and T. Dettlaff. We also thank L. Stodolsky for comments. We acknowledge the Instituto de Astrofísica for providing all infrastructure on the Roque de los Muchachos in La Palma. The support of the German Bundesministerium für Bildung, Wissenschaft, Forschung und Technologie and Max-Planck-Gesellschaft, the Italian INFN and INAF, the Swiss Schweizerische Nationalfonds, and Spanish Ministerio de Ciencia e Innovación is acknowledged. This work was also supported by ETH research grant TH 34/043, by the Polish Ministertwo Nauki i Szkolnictwa Wyzszego grant N N203 390834, and by the Young Investigators Program of the Helmholtz Gemeinschaft.

Supporting Online Material

www.sciencemag.org/cgi/content/full/1164718/DC1
 SOM Text

Figs. S1 to S11
 References

15 August 2008; accepted 8 October 2008

Published online 16 October 2008;

10.1126/science.1164718

Include this information when citing this paper.

List of authors and affiliations:

E. Aliu,¹ H. Anderhub,² L. A. Antonelli,³ P. Antoran,⁴ M. Backes,⁵ C. Baixeras,⁶ J. A. Barrio,⁴ H. Bartko,⁷ D. Bastieri,⁸ J. K. Becker,⁵ W. Bednarek,⁹ K. Berger,¹⁰ E. Bernardini,¹¹ C. Bigongiari,⁸†

A. Biland,² R. K. Bock,^{7,8} G. Bonnoi,¹² P. Bordes,¹³ V. Bosch-Ramon,¹³ T. Bretz,¹⁰ I. Britvitch,² M. Camara,⁴ E. Carmona,⁷ A. Chilingarian,¹⁴ S. Commichau,² J. L. Contreras,⁴ J. Cortina,¹ M. T. Costado,^{15,16} S. Covino,³ V. Curtef,⁵ F. Dazzi,⁹ A. De Angelis,¹⁷ E. De Cea del Pozo,¹⁸ R. de los Reyes,⁴ B. De Lotto,¹⁷ M. De Maria,¹⁷ F. De Sabata,¹⁷ C. Delgado Mendez,¹⁵ A. Dominguez,¹⁹ D. Dörner,¹⁰ M. Doro,⁸ D. Elsässer,¹⁰ M. Errando,¹ M. Fagiolini,¹² D. Ferenc,²⁰ E. Fernandez,¹ R. Firpo,¹ M. V. Fonseca,⁴ L. Font,⁶ N. Galante,⁷ R. J. Garcia Lopez,^{15,16} M. Garzarczyk,⁷ M. Gaug,¹⁵ F. Goebel,⁷ D. Hadash,⁵ M. Hayashida,⁷ A. Herrero,^{15,16} D. Höhne,¹⁰ J. Hose,⁷ C. C. Hsu,⁷ S. Huber,¹⁰ T. Jogler,⁷ D. Kranich,² A. La Barbera,³ A. Laille,²⁰ E. Leonardo,¹² E. Lindfors,²¹ S. Lombardi,⁸ F. Longo,¹⁷ M. Lopez,⁸† E. Lorenz,²⁷ P. Majumdar,⁷ G. Maneva,²⁷ N. Mankuzhiyil,¹⁷ K. Mannheim,¹⁰ L. Maraschi,³ M. Mariotti,⁵ M. Martinez,² D. Mazin,¹ M. Meucci,¹² M. Meyer,¹⁰ J. M. Miranda,⁴ R. Mirzoyan,⁷ M. Moles,¹⁹ A. Moralejo,¹ D. Nieto,⁴ K. Nilsson,²¹ J. Ninkovic,⁷ N. Otte,^{23,7}†§ I. Oya,⁴ R. Paoletti,¹² J. M. Paredes,¹³ M. Pasanen,²¹ D. Pascoli,⁸ F. Pauss,² R. G. Pegna,¹² M. A. Perez-Torres,¹⁹ M. Persic,²⁴ L. Peruzzo,⁸ A. Piccioli,¹² F. Prada,¹⁹ E. Prandini,⁸ N. Puchades,¹ A. Raymers,¹⁴ W. Rhode,⁵ M. Ribó,¹³ J. Rico,^{1,25} M. Rissi,²† A. Robert,⁶ S. Rügamer,¹⁰ A. Saggion,⁸ T. Y. Saito,⁷ M. Salvati,³ M. Sanchez-Conde,¹⁹ P. Sartori,⁸ K. Satallecka,¹¹ V. Scalzotto,⁸ V. Scapin,¹⁷ T. Schweizer,⁷† M. Shayduk,⁷† K. Shinozaki,⁷ S. N. Shore,²⁶ N. Sidro,¹ A. Sierpowska-Bartosik,¹⁸ A. Sillanpää,²¹ D. Sobczynska,⁹ F. Spanier,¹⁰ A. Stamerra,¹² L. S. Stark,² L. Takalo,²¹ F. Tavecchio,³ P. Temnikov,²² D. Tescaro,¹ M. Teshima,⁷ M. Tluczykont,¹¹ D. F. Torres,^{18,25} N. Turini,¹² H. Vankov,²² A. Venturini,⁸ V. Vitale,¹⁷ R. M. Wagner,⁷ W. Wittek,⁷ V. Zabalza,¹³ F. Zandanel,¹⁹ R. Zanin,¹ J. Zapatero,⁵ O. C. de Jager,²⁷|| E. de Ona Wilhelmi¹||¶

¹Institut de Física d'Altes Energies, Edifici Cn, Campus Universitat Autònoma de Barcelona E-08193 Bellaterra, Spain. ²Eidgenössische Technische Hochschule (ETH), Zürich CH-8093, Switzerland. ³L'Istituto Nazionale di Astrofisica (INAF), I-00136 Rome, Italy. ⁴Universidad Complutense, E-28040 Madrid, Spain. ⁵Technische Universität Dortmund, D-44221 Dortmund, Germany. ⁶Universitat Autònoma de Barcelona, E-08193 Bellaterra,

Spain. ⁷Max-Planck-Institut für Physik, D-80805 München, Germany. ⁸Università di Padova and Istituto Nazionale di Fisica Nucleare (INFN), I-35131 Padova, Italy. ⁹University of Lodz, PL-90236 Lodz, Poland. ¹⁰Universität Würzburg, D-97074 Würzburg, Germany. ¹¹Deutsches Elektronen Synchrotron, D-15738 Zeuthen, Germany. ¹²Università di Siena and INFN Pisa, I-53100 Siena, Italy. ¹³Universitat de Barcelona, Institut de Ciències del Cosmos (ICC)/Institut d'Estudis Espacials de Catalunya (IEEC), E-08028 Barcelona, Spain. ¹⁴Yerevan Physics Institute, AM-375036 Yerevan, Armenia. ¹⁵Instituto de Astrofísica de Canarias, E-38200, La Laguna, Tenerife, Spain. ¹⁶Departamento de Astrofísica, Universidad, E-38206 La Laguna, Tenerife, Spain. ¹⁷Università di Udine and INFN Trieste, I-33100 Udine, Italy. ¹⁸IEEC-Consejo Superior de Investigaciones Científicas (CSIC), E-08193 Bellaterra, Spain. ¹⁹Instituto de Astrofísica de Andalucía (CSIC), E-18080 Granada, Spain. ²⁰University of California at Davis, Davis, CA 95616-8677, USA. ²¹Tuorla Observatory, Turku University, FI-21500 Piikkiö, Finland. ²²Institute for Nuclear Research and Nuclear Energy, BG-1784 Sofia, Bulgaria. ²³Humboldt-Universität zu Berlin, D-12489 Berlin, Germany. ²⁴INAF/Osservatorio Astronomico and INFN, I-34143 Trieste, Italy. ²⁵Institució Catalana de Recerca i Estudis Avançats, E-08010 Barcelona, Spain. ²⁶Università di Pisa and INFN Pisa, I-56126 Pisa, Italy. ²⁷Unit for Space Physics, Northwest University, Potchefstroom 2520, South Africa.

†Present address: Instituto de Física Corpuscular, CSIC-Universitat de València, E-46101 Valencia, Spain.

‡To whom correspondence should be addressed. E-mail: tschweiz@mppmu.mpg.de (T.S.); nepomake@scipp.ucsc.edu (N.O.); Michael.Rissi@phys.ethz.ch (M.R.); shayduk@mppmu.mpg.de (M.S.); marcos.lopezmoya@pd.infn.it (M.L.M.)

§Present address: Santa Cruz Institute for Particle Physics, University of California, Santa Cruz, CA 95064, USA.

||These authors are not members of the MAGIC Collaboration.

¶Present address: Astroparticule et Cosmologie, CNRS, Université Paris, F-75205 Paris Cedex 13, France.

Ab Initio Determination of Light Hadron Masses

S. Dürr,¹ Z. Fodor,^{1,2,3} J. Frison,⁴ C. Hoelbling,^{2,3,4} R. Hoffmann,² S. D. Katz,^{2,3} S. Krieg,² T. Kurth,² L. Lellouch,⁴ T. Lippert,^{2,5} K. K. Szabo,^{2,5} G. Vulvert⁴

More than 99% of the mass of the visible universe is made up of protons and neutrons. Both particles are much heavier than their quark and gluon constituents, and the Standard Model of particle physics should explain this difference. We present a full ab initio calculation of the masses of protons, neutrons, and other light hadrons, using lattice quantum chromodynamics. Pion masses down to 190 mega-electron volts are used to extrapolate to the physical point, with lattice sizes of approximately four times the inverse pion mass. Three lattice spacings are used for a continuum extrapolation. Our results completely agree with experimental observations and represent a quantitative confirmation of this aspect of the Standard Model with fully controlled uncertainties.

The Standard Model of particle physics predicts a cosmological, quantum chromodynamics (QCD)-related smooth transition between a high-temperature phase dominated by quarks and gluons and a low-temperature phase dominated by hadrons. The very large energy densities at the high temperatures of the early universe have essentially disappeared through expansion and cooling. Nevertheless, a fraction of this energy is carried today by quarks and gluons, which are confined into protons and neutrons. According to the mass-energy equivalence $E = mc^2$, we experience this energy as mass. Because more than 99% of the mass of ordinary matter comes from protons and neutrons, and in turn about 95% of

their mass comes from this confined energy, it is of fundamental interest to perform a controlled ab initio calculation based on QCD to determine the hadron masses.

QCD is a generalized version of quantum electrodynamics (QED), which describes the electromagnetic interactions. The Euclidean Lagrangian with gauge coupling g and a quark mass of m can be written as $\mathcal{L} = -1/(2g^2)\text{Tr}F_{\mu\nu}F_{\mu\nu} + \bar{\psi}[\gamma_{\mu}(\partial_{\mu} + A_{\mu}) + m]\psi$, where $F_{\mu\nu} = \partial_{\mu}A_{\nu} - \partial_{\nu}A_{\mu} + [A_{\mu}, A_{\nu}]$. In electrodynamics, the gauge potential A_{μ} is a real valued field, whereas in QCD it is a 3×3 matrix field. Consequently, the commutator in $F_{\mu\nu}$ vanishes in QED but not in QCD. The ψ fields also have an additional "color" index in

QCD, which runs from 1 to 3. Different "flavors" of quarks are represented by independent fermionic fields, with possibly different masses. In the work presented here, a full calculation of the light hadron spectrum in QCD, only three input parameters are required: the light and strange quark masses and the coupling g .

The action S of QCD is defined as the four-volume integral of \mathcal{L} . Green's functions are averages of products of fields over all field configurations, weighted by the Boltzmann factor $\exp(-S)$. A remarkable feature of QCD is asymptotic freedom, which means that for high energies (that is, for energies at least 10 to 100 times higher than that of a proton at rest), the interaction gets weaker and weaker ($1, 2$), enabling perturbative calculations based on a small coupling parameter. Much less is known about the other side, where the coupling gets large, and the physics describing the interactions becomes nonperturbative. To explore the predictions of QCD in this nonperturbative regime, the most systematic approach is to discretize (3) the above Lagrangian

¹John von Neumann-Institut für Computing, Deutsches Elektronen-Synchrotron Zeuthen, D-15738 Zeuthen and Forschungszentrum Jülich, D-52425 Jülich, Germany. ²Bergische Universität Wuppertal, Gausstrasse 20, D-42119 Wuppertal, Germany. ³Institute for Theoretical Physics, Eötvös University, H-1117 Budapest, Hungary. ⁴Centre de Physique Théorique (UMR 6207 du CNRS et des Universités d'Aix-Marseille I, d'Aix-Marseille II et du Sud Toulon-Var, affiliée à la FRUMAM), Case 907, Campus de Luminy, F-13288, Marseille Cedex 9, France. ⁵Jülich Supercomputing Centre, FZ Jülich, D-52425 Jülich, Germany.

on a hypercubic space-time lattice with spacing a , to evaluate its Green's functions numerically and to extrapolate the resulting observables to the continuum ($a \rightarrow 0$). A convenient way to carry out this discretization is to place the fermionic variables on the sites of the lattice, whereas the gauge fields are treated as 3×3 matrices connecting these sites. In this sense, lattice QCD is a classical four-dimensional statistical physics system.

Calculations have been performed using the quenched approximation, which assumes that the fermion determinant (obtained after integrating over the ψ fields) is independent of the gauge field. Although this approach omits the most computationally demanding part of a full QCD calculation, a thorough determination of the quenched spectrum took almost 20 years. It

was shown (4) that the quenched theory agreed with the experimental spectrum to approximately 10% for typical hadron masses and demonstrated that systematic differences were observed between quenched and two-flavor QCD beyond that level of precision (4, 5).

Including the effects of the light sea quarks has dramatically improved the agreement between experiment and lattice QCD results. Five years ago, a collaboration of collaborations (6) produced results for many physical quantities that agreed well with experimental results. Thanks to continuous progress since then, lattice QCD calculations can now be performed with light sea quarks whose masses are very close to their physical values (7) (though in quite small volumes). Other calculations, which include these sea-quark

effects in the light hadron spectrum, have also appeared in the literature (8–16). However, all of these studies have neglected one or more of the ingredients required for a full and controlled calculation. The five most important of those are, in the order that they will be addressed below:

1) The inclusion of the up (u), down (d), and strange (s) quarks in the fermion determinant with an exact algorithm and with an action whose universality class is QCD. For the light hadron spectrum, the effects of the heavier charm, bottom, and top quarks are included in the coupling constant and light quark masses.

2) A complete determination of the masses of the light ground-state, flavor nonsinglet mesons and octet and decuplet baryons. Three of these are used to fix the masses of the isospin-averaged light (m_{ud}) and strange (m_s) quark masses and the overall scale in physical units.

3) Large volumes to guarantee small finite-size effects and at least one data point at a significantly larger volume to confirm the smallness of these effects. In large volumes, finite-size corrections to the spectrum are exponentially small (17, 18). As a conservative rule of thumb, $M_\pi L \geq 4$, with M_π the pion mass and L the lattice size, guarantees that finite-volume errors in the spectrum are around or below the percent level (19). Resonances require special care. Their finite volume behavior is more involved. The literature provides a conceptually satisfactory framework for these effects (20, 21), which should be included in the analysis.

4) Controlled interpolations and extrapolations of the results to physical m_{ud} and m_s (or eventually directly simulating at these mass values). Although interpolations to physical m_s , corresponding to $M_K \cong 495$ MeV, are straightforward, the extrapolations to the physical value of

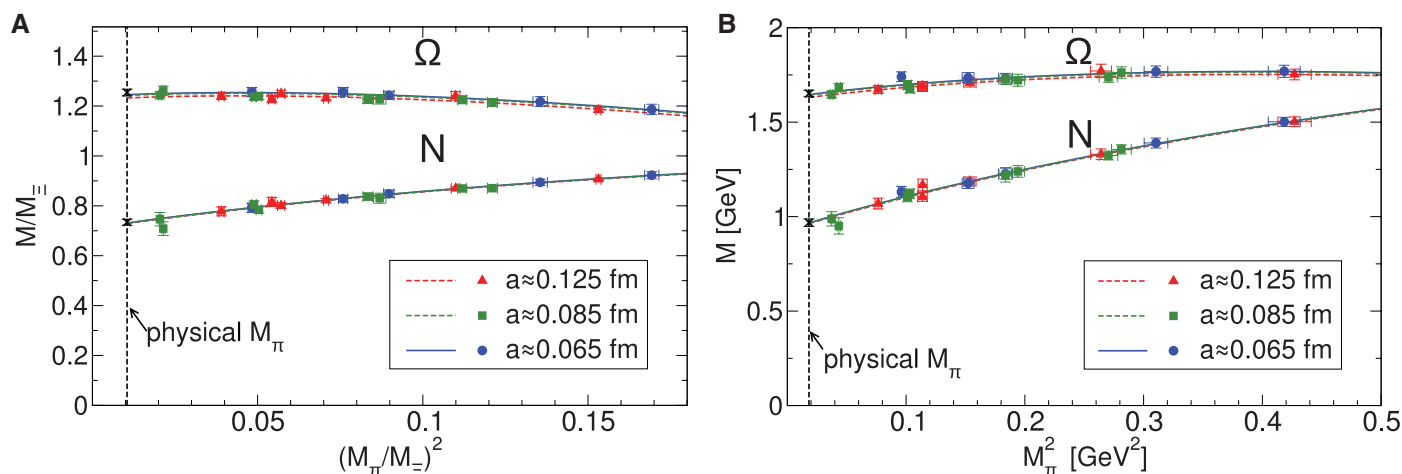
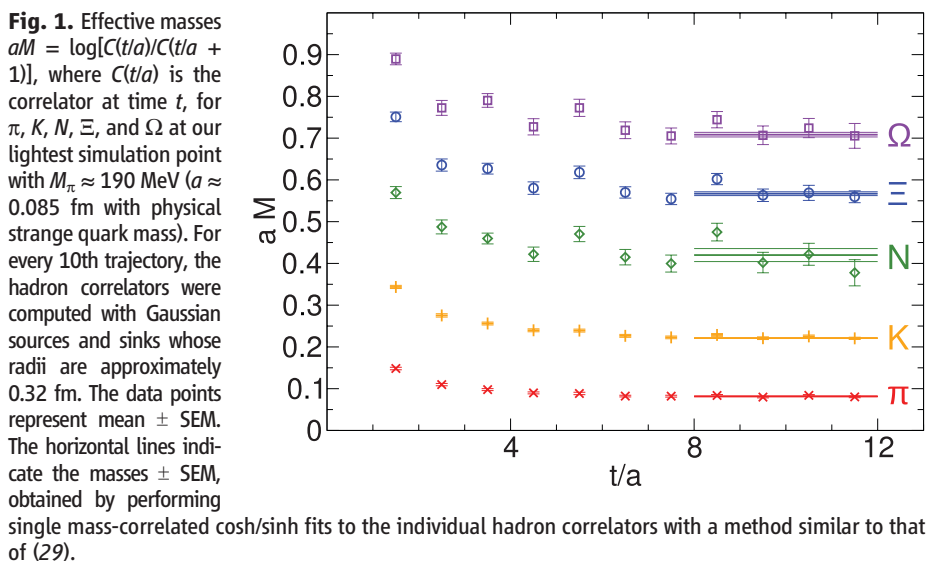


Fig. 2. Pion mass dependence of the nucleon (N) and Ω for all three values of the lattice spacing. (A) Masses normalized by M_Ξ , evaluated at the corresponding simulation points. (B) Masses in physical units. The scale in this case is set by M_Ξ at the physical point. Triangles on dotted lines correspond to $a \approx 0.125$ fm, squares on dashed lines to $a \approx 0.085$ fm, and circles on solid lines to $a \approx 0.065$ fm. The points were obtained by interpolating the lattice results to the physical m_s (defined by setting $2M_K^2 - M_\pi^2$ to its physical value).

The curves are the corresponding fits. The crosses are the continuum extrapolated values in the physical pion mass limit. The lattice-spacing dependence of the results is barely significant statistically despite the factor of 3.7 separating the squares of the largest ($a \approx 0.125$ fm) and smallest ($a \approx 0.065$ fm) lattice spacings. The $\chi^2/\text{degrees of freedom}$ values of the fits in (A) are 9.46/14 (Ω) and 7.10/14 (N), whereas those of the fits in (B) are 10.6/14 (Ω) and 9.33/14 (N). All data points represent the mean \pm SEM.

m_{ud} , corresponding to $M_\pi \cong 135$ MeV, are difficult. They need computationally intensive calculations, with M_π reaching down to 200 MeV or less.

5) Controlled extrapolations to the continuum limit, requiring that the calculations be performed at no less than three values of the lattice spacing, in order to guarantee that the scaling region is reached.

Our analysis includes all five ingredients listed above, thus providing a calculation of the light hadron spectrum with fully controlled systematics as follows.

1) Owing to the key statement from renormalization group theory that higher-dimension, local operators in the action are irrelevant in the continuum limit, there is, in principle, an unlimited freedom in choosing a lattice action. There is no consensus regarding which action would offer the most cost-effective approach to the continuum limit and to physical m_{ud} . We use an action that improves both the gauge and fermionic sectors and heavily suppresses non-physical, ultraviolet modes (19). We perform a series of 2 + 1 flavor calculations; that is, we include degenerate u and d sea quarks and an additional s sea quark. We fix m_s to its approximate physical value. To interpolate to the physical value, four of our simulations were repeated with a slightly different m_s . We vary m_{ud} in a range that extends down to $M_\pi \approx 190$ MeV.

2) QCD does not predict hadron masses in physical units: Only dimensionless combinations (such as mass ratios) can be calculated. To set the overall physical scale, any dimensionful observable can be used. However, practical issues influence this choice. First of all, it should be a quantity that can be calculated precisely and whose experimental value is well known. Second, it should have a weak dependence on m_{ud} , so that its chiral behavior does not interfere with that of other observables. Because we are considering spectral quantities here, these two conditions should guide our choice of the particle whose mass will set the scale. Furthermore, the particle should not decay under the strong interaction. On the one hand, the larger the strange content of the particle, the more precise the mass determination and the weaker the dependence on m_{ud} . These facts support the use of the Ω baryon, the particle with the highest strange content. On the other hand, the determination of baryon decuplet masses is usually less precise than those of the octet. This observation would suggest that the Ξ baryon is appropriate. Because both the Ω and Ξ baryon are reasonable choices, we carry out two analyses, one with M_Ω (the Ω set) and one with M_Ξ (the Ξ set). We find that for all three gauge couplings, $6/g^2 = 3.3, 3.57, \text{ and } 3.7$, both quantities give consistent results, namely $a \approx 0.125, 0.085, \text{ and } 0.065$ fm, respectively. To fix the bare quark masses, we use the mass ratio pairs $M_\pi/M_\Omega, M_K/M_\Omega$ or $M_\pi/M_\Xi, M_K/M_\Xi$. We determine the masses of the baryon octet (N, Σ, Λ, Ξ) and decuplet ($\Delta, \Sigma^*, \Xi^*, \Omega$) and those members of the light pseudoscalar (π, K) and

vector meson (ρ, K^*) octets that do not require the calculation of disconnected propagators. Typical effective masses are shown in Fig. 1.

3) Shifts in hadron masses due to the finite size of the lattice are systematic effects. There are two different effects, and we took both of them into account. The first type of volume dependence is related to virtual pion exchange between the different copies of our periodic system, and it decreases exponentially with $M_\pi L$. Using $M_\pi L \gtrsim 4$ results in masses which coincide, for all practical purposes, with the infinite volume results [see results, for example, for pions (22) and for baryons (23, 24)]. Nevertheless, for one of our simulation points, we used several volumes and determined the volume dependence, which was included as a (negligible) correction at all points (19). The second type of volume dependence exists only for resonances. The coupling between the resonance state and its decay products leads to a nontrivial-level structure in finite volume. Based on (20, 21), we calculated the corrections necessary to reconstruct the resonance masses from the finite volume ground-state energy and included them in the analysis (19).

4) Though important algorithmic developments have taken place recently [for example

(25, 26) and for our setup (27)], simulating directly at physical m_{ud} in large enough volumes, which would be an obvious choice, is still extremely challenging numerically. Thus, the standard strategy consists of performing calculations at a number of larger m_{ud} and extrapolating the results to the physical point. To that end, we use chiral perturbation theory and/or a Taylor expansion around any of our mass points (19).

5) Our three-flavor scaling study (27) showed that hadron masses deviate from their continuum values by less than approximately 1% for lattice spacings up to $a \approx 0.125$ fm. Because the statistical errors of the hadron masses calculated in the present paper are similar in size, we do not expect significant scaling violations here. This is confirmed by Fig. 2. Nevertheless, we quantified and removed possible discretization errors by a combined analysis using results obtained at three lattice spacings (19).

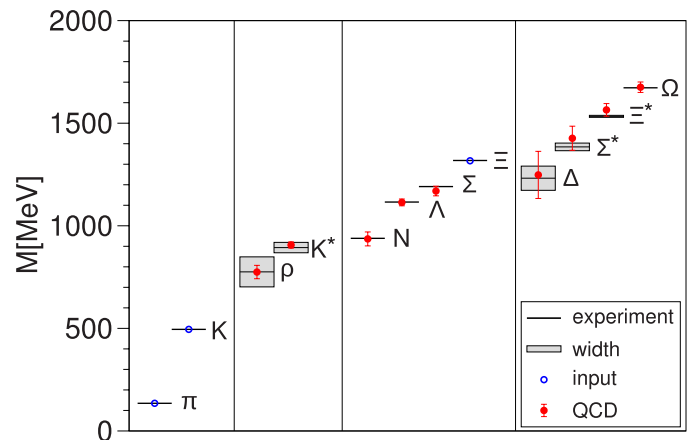
We performed two separate analyses, setting the scale with M_Ξ and M_Ω . The results of these two sets are summarized in Table 1. The Ξ set is shown in Fig. 3. With both scale-setting procedures, we find that the masses agree with the hadron spectrum observed in nature (28).

Thus, our study strongly suggests that QCD is the theory of the strong interaction, at low

Table 1. Spectrum results in giga-electron volts. The statistical (SEM) and systematic uncertainties on the last digits are given in the first and second set of parentheses, respectively. Experimental masses are isospin-averaged (19). For each of the isospin multiplets considered, this average is within at most 3.5 MeV of the masses of all of its members. As expected, the octet masses are more accurate than the decuplet masses, and the larger the strange content, the more precise is the result. As a consequence, the Δ mass determination is the least precise.

| X | Experimental (28) | M_X (Ξ set) | M_X (Ω set) |
|------------|-------------------|--------------------|-----------------------|
| ρ | 0.775 | 0.775 (29) (13) | 0.778 (30) (33) |
| K^* | 0.894 | 0.906 (14) (4) | 0.907 (15) (8) |
| N | 0.939 | 0.936 (25) (22) | 0.953 (29) (19) |
| Λ | 1.116 | 1.114 (15) (5) | 1.103 (23) (10) |
| Σ | 1.191 | 1.169 (18) (15) | 1.157 (25) (15) |
| Ξ | 1.318 | 1.318 | 1.317 (16) (13) |
| Δ | 1.232 | 1.248 (97) (61) | 1.234 (82) (81) |
| Σ^* | 1.385 | 1.427 (46) (35) | 1.404 (38) (27) |
| Ξ^* | 1.533 | 1.565 (26) (15) | 1.561 (15) (15) |
| Ω | 1.672 | 1.676 (20) (15) | 1.672 |

Fig. 3. The light hadron spectrum of QCD. Horizontal lines and bands are the experimental values with their decay widths. Our results are shown by solid circles. Vertical error bars represent our combined statistical (SEM) and systematic error estimates. π, K , and Ξ have no error bars, because they are used to set the light quark mass, the strange quark mass and the overall scale, respectively.



energies as well, and furthermore that lattice studies have reached the stage where all systematic errors can be fully controlled. This will prove important in the forthcoming era in which lattice calculations will play a vital role in unraveling possible new physics from processes that are interlaced with QCD effects.

References and Notes

1. D. J. Gross, F. Wilczek, *Phys. Rev. Lett.* **30**, 1343 (1973).
2. H. D. Politzer, *Phys. Rev. Lett.* **30**, 1346 (1973).
3. K. G. Wilson, *Phys. Rev. D Part. Fields* **10**, 2445 (1974).
4. S. Aoki *et al.*, *Phys. Rev. Lett.* **84**, 238 (2000).
5. S. Aoki *et al.*, *Phys. Rev. D Part. Fields* **67**, 034503 (2003).
6. C. T. H. Davies *et al.*, *Phys. Rev. Lett.* **92**, 022001 (2004).
7. S. Aoki *et al.*, <http://arxiv.org/abs/0807.1661> (2008).
8. C. W. Bernard *et al.*, *Phys. Rev. D Part. Fields* **64**, 054506 (2001).
9. C. Aubin *et al.*, *Phys. Rev. D Part. Fields Gravit. Cosmol.* **70**, 094505 (2004).

10. N. Ukita *et al.*, *Proc. Sci.* **LAT2007**, 138 (2007).
11. M. Gockeler *et al.*, *Proc. Sci.* **LAT2007**, 129 (2007).
12. D. J. Antonio *et al.*, *Phys. Rev. D Part. Fields Gravit. Cosmol.* **75**, 114501 (2007).
13. A. Walker-Loud *et al.*, <http://arxiv.org/abs/0806.4549> (2008).
14. L. Del Debbio, L. Giusti, M. Luscher, R. Petronzio, N. Tantalo, *J. High Energy Phys.* **02**, 056 (2007).
15. C. Alexandrou *et al.*, <http://arxiv.org/abs/0803.3190> (2008).
16. J. Noaki *et al.*, *Proc. Sci.* **LAT2007**, 126 (2007).
17. M. Luscher, *Commun. Math. Phys.* **104**, 177 (1986).
18. M. Luscher, *Commun. Math. Phys.* **105**, 153 (1986).
19. See supporting material on Science Online.
20. M. Luscher, *Nucl. Phys. B* **354**, 531 (1991).
21. M. Luscher, *Nucl. Phys. B* **364**, 237 (1991).
22. G. Colangelo, S. Durr, *Eur. Phys. J. C* **33**, 543 (2004).
23. A. Ali Khan *et al.*, *Nucl. Phys. B* **689**, 175 (2004).
24. B. Orth, T. Lippert, K. Schilling, *Phys. Rev. D Part. Fields Gravit. Cosmol.* **72**, 014503 (2005).
25. M. A. Clark, *Proc. Sci.* **LAT2006**, 004 (2006).
26. W. M. Wilcox, *Proc. Sci.* **LAT2007**, 025 (2007).
27. S. Durr *et al.*, <http://arxiv.org/abs/0802.2706> (2008).

28. W. M. Yao *et al.*, *J. Phys.* **G33**, 1 (2006).
29. C. Michael, A. McKerrell, *Phys. Rev. D Part. Fields* **51**, 3745 (1995).
30. Computations were performed on the Blue Gene supercomputers at FZ Jülich and at IDRIS and on clusters at Wuppertal and CPT. This work is supported in part by European Union (EU) grant I3HP; Országos Tudományos Kutatási Alapprogramok grant AT049652; Deutsche Forschungsgemeinschaft grants FO 502/1-2 and SFB-TR 55; EU grants RTN contract MRTN-CT-2006-035482 (FLAVIANet) and (FP7/2007-2013)/ERC no. 208740; and the CNRS's GDR grant 2921. Useful discussions with J. Charles and M. Knecht are acknowledged.

Supporting Online Material

www.sciencemag.org/cgi/content/full/322/5905/1224/DC1

SOM Text

Figs. S1 to S5

Tables S1 and S2

References

14 July 2008; accepted 1 October 2008

10.1126/science.1163233

4D Imaging of Transient Structures and Morphologies in Ultrafast Electron Microscopy

Brett Barwick, Hyun Soon Park, Oh-Hoon Kwon, J. Spencer Baskin, Ahmed H. Zewail*

With advances in spatial resolution reaching the atomic scale, two-dimensional (2D) and 3D imaging in electron microscopy has become an essential methodology in various fields of study. Here, we report 4D imaging, with in situ spatiotemporal resolutions, in ultrafast electron microscopy (UEM). The ability to capture selected-area-image dynamics with pixel resolution and to control the time separation between pulses for temporal cooling of the specimen made possible studies of fleeting structures and morphologies. We demonstrate the potential for applications with two examples, gold and graphite. For gold, after thermally induced stress, we determined the atomic structural expansion, the nonthermal lattice temperature, and the ultrafast transients of warping/bulging. In contrast, in graphite, striking coherent transients of the structure were observed in both image and diffraction, directly measuring, on the nanoscale, the longitudinal resonance period governed by Young's elastic modulus. The success of these studies demonstrates the promise of UEM in real-space imaging of dynamics.

Electrons, because of their wave-particle duality, can be accelerated to have picometer wavelength and focused to image in real space (*I*). With the impressive advances made in transmission electron microscopy (TEM), augmented by scanning and aberration-correction features, it is now possible to image with high resolution (2–7), reaching the sub-angstrom scale. Together with the progress made in electron crystallography, tomography, and single-particle imaging (8–13), today the electron microscope in different variants of two-dimensional (2D) and 3D recordings has become a central tool in many fields, from materials science to biology (14–16). For all conventional microscopes, the electrons are generated either thermally by heating the

cathode or by field emission, and as such the electron beam is made of random single-electron bursts with no control over the temporal behavior. In these microscopes, time resolution of milliseconds or longer, being limited by the video rate of the detector, can be achieved, while maintaining the high spatial resolution, as demonstrated in environmental-TEM studies (17).

Ultrafast imaging, using pulsed photoelectron packets, provides opportunities for studying, in real space, the elementary processes of structural and morphological changes. In electron diffraction, ultrashort time resolution is possible (18), but the data are recorded in reciprocal space. With nanosecond and submicron image resolutions (19, 20) limited by space charge, ultrashort processes cannot be observed. To achieve ultrafast resolution in microscopy, the concept of single-electron pulse imaging (18) was realized as a key to the elimination of the Coulomb repulsion between electrons while maintaining the high temporal and spatial resolutions. As long

as the number of electrons in each pulse is below the space-charge limit, the packet can have a few or tens of electrons, and the temporal resolution is still determined by the femtosecond (fs) optical pulse duration and the energy uncertainty, which is also on the fs time scale (21), and the spatial resolution is atomic scale (22). However, the goal of full-scale dynamic imaging can be attained only when, in the microscope, the problems of in situ high-spatiotemporal resolution for selected image areas and of heat dissipation (for reversible processes) are overcome.

Here, we present the methodology of ultrafast imaging with applications in studies of structural and morphological changes in single-crystal gold and graphite films, which exhibit entirely different dynamics. For both, the changes were initiated by in situ fs impulsive heating, while image frames and diffraction patterns were recorded in the microscope at well-defined times after the temperature jump. The time axis in the microscope is independent of the response time of the detector, and it is established using a variable delay-line arrangement; a 1- μm change in optical path of the initiating (clocking) pulse corresponds to a time step of 3.3 fs.

Shown in Fig. 1 is a picture of the second-generation ultrafast electron microscope (UEM-2) built at the California Institute of Technology (Caltech). The integration of two laser systems to a modified electron microscope is indicated in the figure, together with a representative image showing the resolution of a 3.4 Å lattice spacing obtained in UEM without the field-emission-gun (FEG) arrangement of conventional TEM. In the figure, the fs laser system is used to generate the single-electron packets, whereas the ns laser system was used for both single-shot and stroboscopic recordings (23). In the single-electron mode of operation, as in UEM-1 (24), the coherence volume is well defined and appropriate for image formation in repetitive events (25). The dynamics are fully reversible, retracing an identical evolution after each initiating laser pulse; each image is constructed stroboscopically, in seconds,

Physical Biology Center for Ultrafast Science and Technology, Arthur Amos Noyes Laboratory of Chemical Physics, California Institute of Technology, Pasadena, CA 91125, USA.

*To whom correspondence should be addressed. E-mail: zewail@caltech.edu